ACS APPLIED MATERIALS & INTERFACES

Research Article

www.acsami.org

Genetically Programmed Clusters of Gold Nanoparticles for Cancer Cell-Targeted Photothermal Therapy

Mi Hwa Oh,[†] Jeong Heon Yu,[‡] Insu Kim,[‡] and Yoon Sung Nam*[,‡,§]

[†]Department of Biological Sciences, [‡]Department of Materials Science and Engineering, [§]KAIST Institute for NanoCentury (KINC CNiT), Korea Advanced Institute of Science and Technology (KAIST), 291 Daehak-ro, Yuseong-gu, Daejeon 305-701, Republic of Korea

Supporting Information

ABSTRACT: Interpretations of the interactions of nanocarriers with biological cells are often complicated by complex synthesis of materials, broad size distribution, and heterogeneous surface chemistry. Herein, the major capsid proteins of an icosahedral T7 phage (55 nm in diameter) are genetically engineered to display a gold-binding peptide and a prostate cancer cell-binding peptide in a tandem sequence. The genetically modified phage attracts gold nanoparticles (AuNPs) to form a cluster of gold nanoparticles (about 70 nanoparticles per phage). The cluster of AuNPs maintains cell-targeting functionality and exhibits excellent dispersion stability in serum. Under a very low light irradiation (60 mW cm^{-2}), only targeted AuNP clusters kill the prostate cancer cells in minutes (not in other cell types), whereas neither nontargeted AuNP clusters nor citrate-stabilized AuNPs cause any significant cell death. The result suggests that the prostate cancer cell-targeted clusters of AuNPs are targeted to only prostate cancer cells and, when illuminated, generate local heating to more efficiently and selectively kill the targeted cancer cells. Our strategy can be generalized to target other types of cells and assemble other kinds of nanoparticles for a broad range of applications.

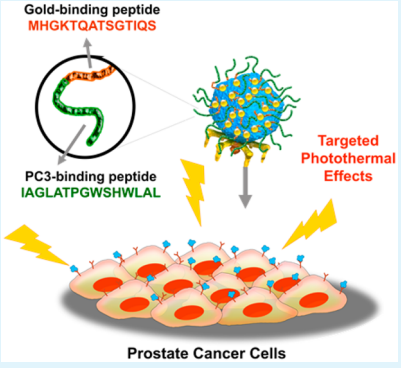

KEYWORDS: *T7 bacteriophage, gold nanoparticles, self-assembly, cancer targeting, photothermal therapy*

Bacteriophages, often called phages, have received growing attention as a well-defined protein-based platform for the assembly of nanostructured functional molecules and materials.[1−5] They are biocompatible, very uniform in size and morphology, and relatively stable at a high temperature, in a wide range of pH, and in the presence of nucleases and proteases.[6,7] Their surface chemistry can be easily controlled by a technique called as "phage display", which is based on genetic modification of phage genomes to express extra peptides on the coat proteins of phages.[1−4] Randomized peptides can be expressed on the coat proteins to produce a phage library. Biopanning is a selection process to identify peptide motifs that exhibit a high binding affinity to specific molecules, proteins, materials, cells, and organs.[8,−10] A filamentous M13 phage has been widely utilized to express short peptides on the coat proteins for peptide-mediated assembly of various materials (e.g., metal, metal oxide, molecular dyes, and carbon nanomaterials) for applications to the production of nanostructured materials for lithium ion batteries, photocatalysis, photovoltaics, and piezoelectric devices.[1−5,11,12]

Phages are particularly attractive for therapeutic and bioimaging applications because a wide range of biomolecular interactions (e.g., antibody−antigen, ligand−receptors, and peptide−peptide interactions) have been studied using phage display.[8,9,13] In this respect, phages can be used as a platform for the delivery of therapeutic and imaging agents because targeting ligands and imaging probes can be easily conjugated to the chemically well-defined surface of phages.[14,15] Recently, Ghosh et al. showed a very promising result on in vivo bioimaging using M13 phages as a delivery carrier.[16] They displayed a SPARC (secreted protein, acidic and rich in cysteine)-binding peptide, SPPTGIN, on the pIII minor coat proteins for prostate cancer targeting and triglutamate on the pVIII major coat protins for templated assembly of iron oxide nanoparticles. The genetically engineered M13 phages were evaluated for magnetic resonance imaging (MRI) of targeted cancer cells in vivo. M13 phages were also utilized to assemble fluorescent single-walled carbon nanotubes (SWNT) by displaying a pH-sensitive SWNT-binding peptide (DSPHTELP) on pVIII for second near-infrared (NIR) window fluorescence imaging.[17] Furthermore, the refactored M13 phage genome, which was redesigned by physical separation of overlapping genetic elements between pIX and pVII, was applied for targeted bioimaging and drug delivery to prostate cancer cells.[18] Despite attractive features of M13 phages as a template for assembly of functional nanomaterials, M13 phages are relatively long (about 1 μm) to penetrate a plasma cell membrane, and only five copies of peptides displayed on pIII are used to target cancer cells.

Received: July 31, 2015
Accepted: September 28, 2015
Published: September 28, 2015

DOI: 10.1021/acsami.5b07029
ACS Appl. Mater. Interfaces 2015, 7, 22578−22586

By comparison, T7 phages can display 415 copies of extra peptides on their capsid shell by simple genetic manipulation, providing a high apparent binding affinity to target molecules and materials via multivalent interactions. In practice, it was demonstrated that T7 phages displaying a RGD motif showed a very strong affinity to human transferrin immobilized on a surface plasmon resonance (SPR) chip.[19] T7 phage has an icosahedral shape with a diameter of about 55 nm, comprising a capsid shell of 10B major capsids (gene 10).[20,21] The size and shape of T7 phages are desirable for intracellular delivery of therapeutic and imaging agents. Another important advantage of T7 phages as a targetable carrier is that a relatively long peptide can be displayed on all of the major coat proteins.

AuNPs have been widely investigated for theranostic and biosensor applications due to their unique optical properties, biocompatibility, and chemical stability.[22] Methods to control the size and morphology of AuNPs and functionalize their surfaces have been well-established for the past decade.[23,24] In particular, the light-to-heat conversion under light illumination at a frequency overlapped with the absorption band of SPR of AuNPs makes them an attractive heat source for hyperthermic damage to cancer cells.[25] Photothermal therapy, also called hyperthermal therapy, is a minimally invasive approach to cancer treatments. Its aims to treat not only a tumor with a small volume in sites where surgery is difficult but also a tumor placed in organs requiring functional preservation such as prostate and uterus. In addition, to enhance the highly intensive and localized hyperthermic effect without damaging normal tissues, photothermal therapy using surface functionalized AuNPs have been investigated.[26] However, commonly used AuNPs have some limitation for photothermal therapy because of their low heating efficiency and a low absorption level within the tissue transmittance spectra.[27] It has been reported that structural parameters of AuNPs (e.g., size and shape) are related to the efficiency of photothermal therapy. Compared to AuNPs, gold nanoshells and gold nanorods exhibited an increased absorption and spectral tunability to a longer wavelength, leading to enhanced photothermal effects in the near-infrared region.[28] However, the fabrication of a thin gold shell of 3 to 8 nm thick, exhibiting the maximal absorbance, is very difficult to control. As an alternative way, the assembly of AuNPs on polymer templates by dipole−dipole interactions was employed to induce the red shift of their absorption spectrum.[29] It was also reported that pH-responsive aggregation of AuNPs in an acidic condition enhanced photothermal effects with a low illumination threshold.[30] Furthermore, theoretical simulations characterized nanocluster structures to achieve the maximal SPR absorption for efficient photothermal effects.[31] These studies concluded that the clusterization of AuNPs without particle intersection can be an effective route to efficient photothermal therapy.

In this study, we introduce genetically modified T7 phages as a multifunctional template to self-assemble AuNPs to hollow nanoclusters for cancer-targeted photothermal therapy (Figure 1). To assemble AuNPs on the surface of T7 phages, a 14-amino-acid gold-binding sequence (MHGKTQATSGTIQS) was fused to the major coat 10B protein.[32] The genetically engineered phage is denoted as "**G-phage**". Among several gold-binding peptide sequences, the above sequence was chosen because of a high binding affinity even at a high salt concentration. The dissociation constant (K_d) was 150 pM. The selected gold-binding peptide does not include any cysteine residue, which generally forms a chemical linkage

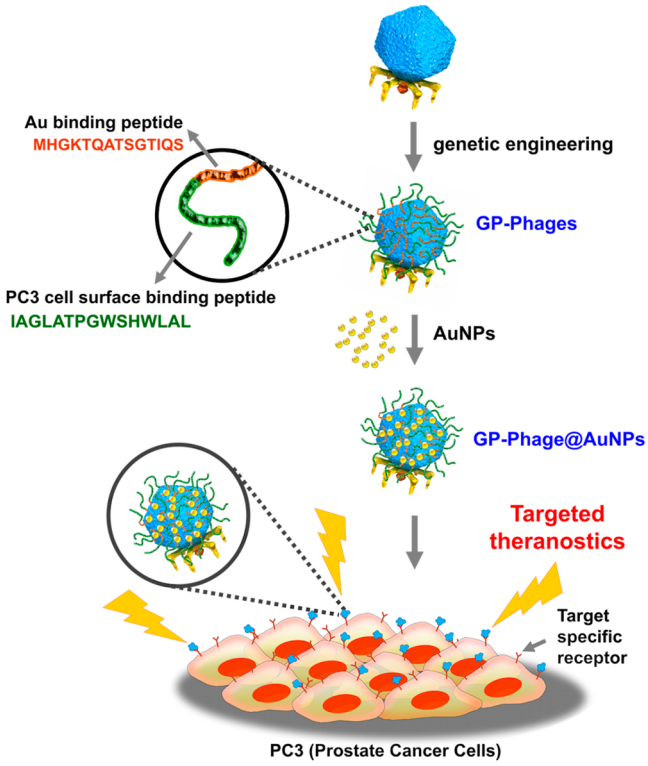

Figure 1. Schematic illustration of cancer-selective photothermal therapy via prostate cancer-targeted intracellular delivery of T7-templated AuNP nanoclusters, where T7 phages are genetically modified to display gold-binding and prostate cancer cell-targeting peptides on the viral surface.

between Au and a thiol group as shown in self-assembled monolayers.[33] On the other hand, the gold-binding peptide contains amino acids with polar hydrophilic side chains including glutamine, serine, and threonine.[32,34] The binding mechanism of such hydroxyl-rich peptides has been investigated, but molecular level details are not yet fully proved, indicating the complex nature of peptide-inorganic surface interactions in an aqueous milieu under ambient conditions. This physisorption process is basically mediated by a combination of multiple interactions, including lattice matching, intermolecular interactions within the peptide, and solvent-surface interactions.[34−36]

RESULTS AND DISCUSSION

To design T7 phages as a hybrid nanocarrier for cancer targeting, a peptide that targets the surface of prostate cancer cells (PC3) was also displayed to each 10B capsid. Although prostate-specific antigen (PSA) and prostate-specific membrane antigen (PSMA) have been used to diagnose prostate cancers, they have relatively a low specificity and do not work for all types of prostate cancers.[37] In this work, a prostate cancer cell-binding peptide (IAGLATPGWSHWLAL), isolated by biopanning from fUSE5 phage display, was introduced along with the gold-binding peptide on the same capsid protein in a tandem arrangement.[38] The DNA sequences encoding gold- and PC3-binding peptides were connected with a tetraglycine linker and ligated into a T7Select 415−1b vector. As control samples, T7 phages that display either the gold-binding peptide or the PC3-binding peptide were also constructed in the same manner. The expression of the external peptides was verified by sequencing

DOI: 10.1021/acsami.5b07029
ACS Appl. Mater. Interfaces 2015, 7, 22578−22586

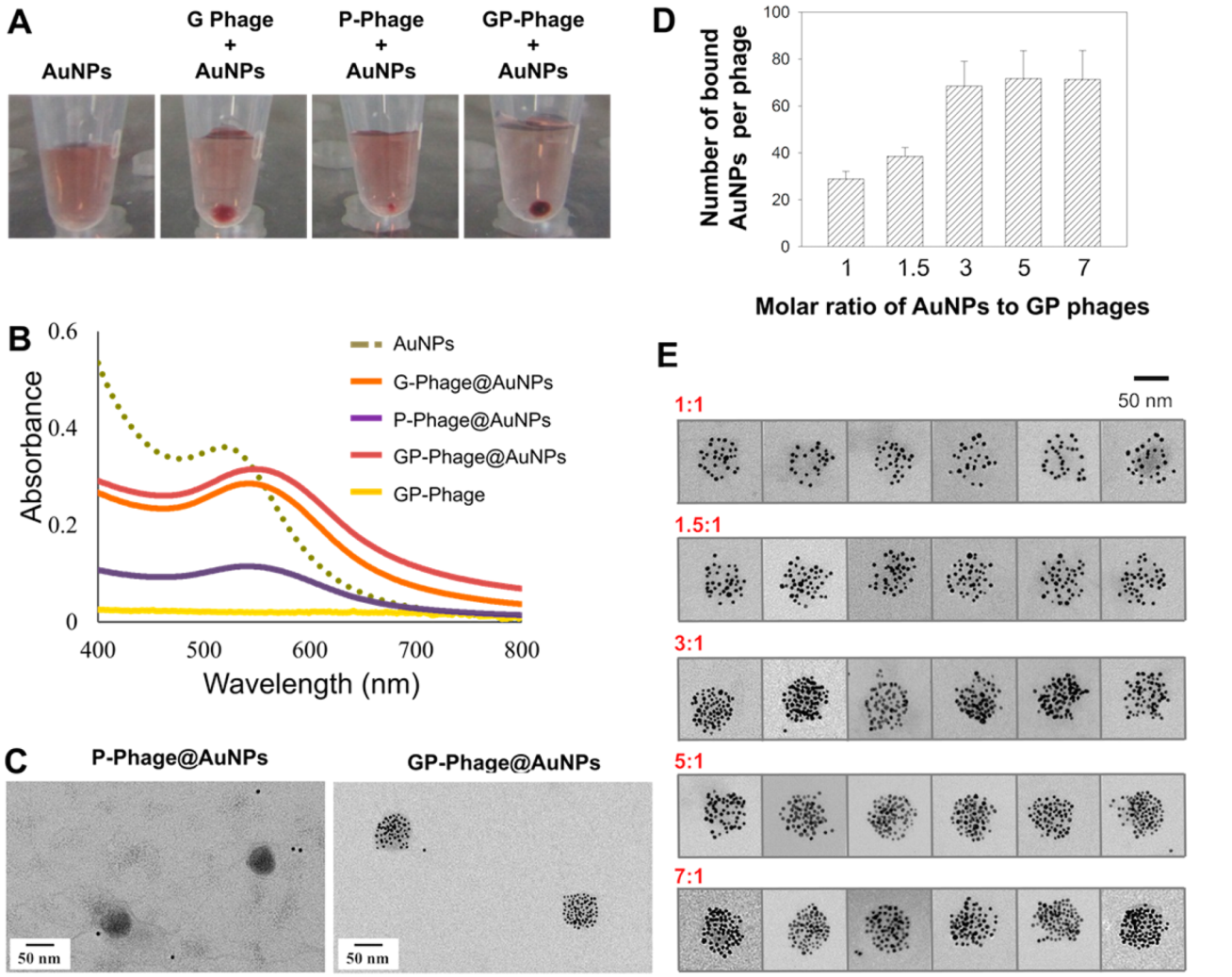

Figure 2. Binding of AuNPs with the recombinant phages. (A) The photograph of engineered phages bearing different genes incubated with AuNPs. The phages presenting peptides having gold binding affinity (G-phage and GP-phage) showed clearly visible precipitates compared to others. (B) Absorption spectrum of various phages with AuNPs. C. TEM images of P-phage@AuNPs and GP-phage@AuNPs. The contrast difference between the images was caused by different exposure time. (D) The average number of AuNPs bound on the capsid of T7 phage at each molar ratio was measured from TEM images. The average number of AuNPs was counted from 15 samples. (E) TEM imagies of GP-phage@AuNPs at each molar ratio of AuNPs to GP-phages. All TEM samples were stained with 1% uranyl acetate.

the PCR products of selected plaques. The phages displaying the PC3-binding peptide are denoted as "**P-phage**", and the ones displaying both of the peptides as "**GP-phage**". The fusion of the peptides to the capsid proteins of T7 phages did not significantly influence on the morphology of phages compared to unmodified ones, as observed by TEM (Figure S1). The amplification rate of G-phage, P-phage, and GP-phage from a 2 L-scale amplification were 2.0×10^{11} pfu mL^{-1}, 2.8×10^{11} pfu mL^{-1}, and 1.9×10^{11} pfu mL^{-1}, respectively. There were no significant differences in terms of an amplification rate compared to that of unmodified T7 phage (2.6×10^{11} pfu mL^{-1}).

The prepared recombinant phages were evaluated in terms of specific binding ability of AuNPs. P-phage containing no gold-binding motif was used as a negative control. Ten microliters of each recombinant T7 phage prepared at a concentration of 2×10^{11} pfu mL^{-1} were mixed with a 50 μL suspension of 5 nm AuNPs (5×10^{13} particles mL^{-1}). After incubation for 20 min, the samples were exposed to the centrifugal force ($2250 \times g$). No precipitation was observed for the control AuNPs suspension and the mixture of AuNPs with P-phage (Figure 2A). On the other hand, reddish precipitation was observed for both of G-phage and GP-phage presumably due to the clusterization of AuNPs on the phages. The precipitates were resuspended in 0.1 mL PBS, and the absorption spectrum of the resuspended samples was measured. The formation of gold clusters on T7 phages resulted in red shift of the SPR peak from 520 nm to about 540 nm with peak broadening (Figure 2B). Free GP-phage without AuNPs did not show any light absorption in the same range of wavelength. Therefore, the red shift of the SPR peak of the clusters of AuNPs on G-phage (denoted 'G-phage@AuNPs') and GP-phage (denoted 'GP-phage@AuNPs') indicates that AuNPs were bound to the recombinant phages via specific interactions with the gold-binding peptide motif displayed on the phages.

The capsid shell of GP-phage was covered by 5 nm AuNPs, whereas P-phage and wild-type phage were not combined with AuNPs (Figure 2C). The number of AuNPs bound to T7 phages was measured from TEM images. Figure 2D shows the average number of AuNPs bound to each GP-phage as a

DOI: 10.1021/acsami.5b07029
ACS Appl. Mater. Interfaces 2015, 7, 22578−22586

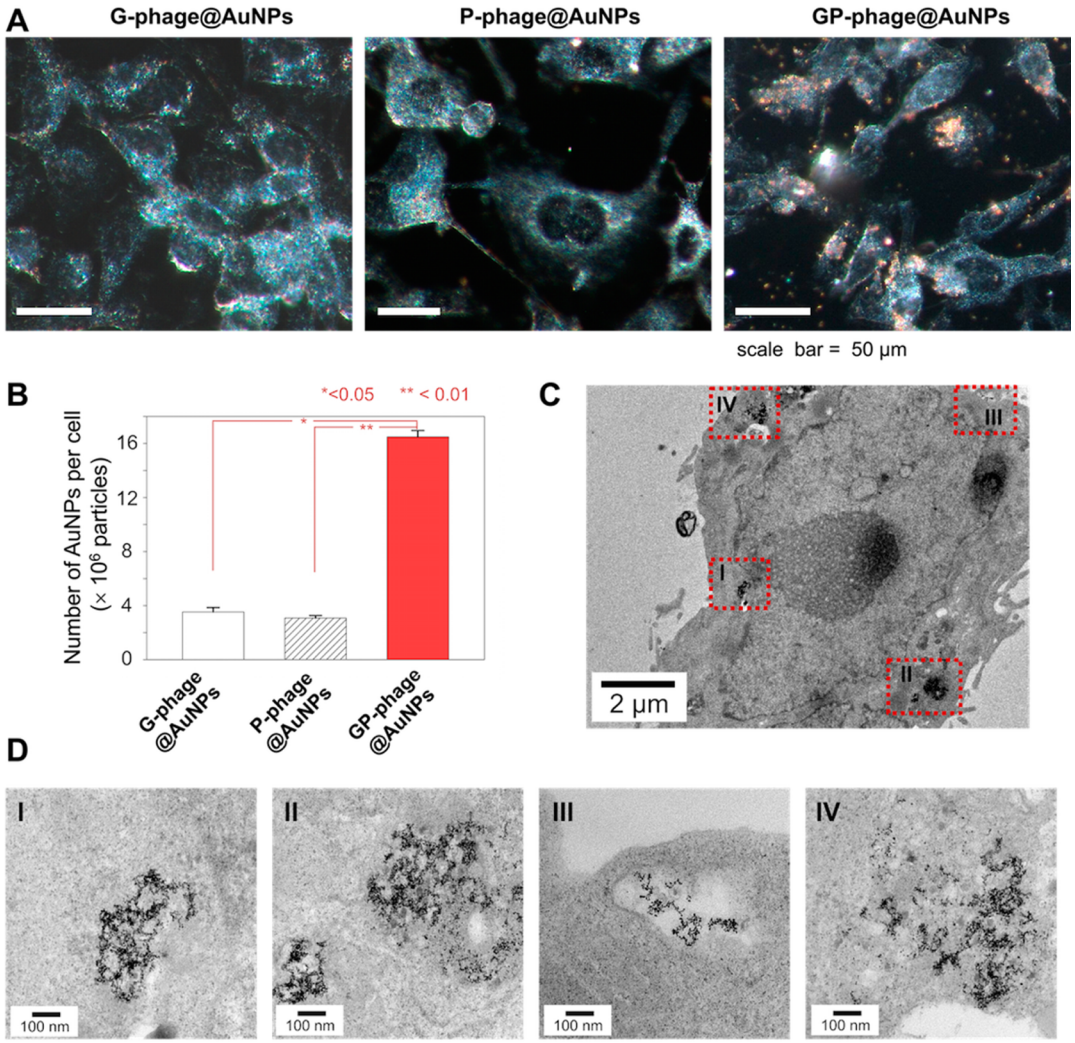

Figure 3. Cellular uptake and distribution of GP-phage@AuNPs into PC3 cells. (A) Dark-field images of GP-phage@AuNPs, P-phage@AuNPs, and GP-phage@AuNPs bound on the cells. (B) The number of AuNPs bound on each recombinant phages taken into PC3 cells was measured using ICP-MS. Significant statistical differences based on analysis of variance were assigned for p-values of <0.05 (*) and <0.01 (**) with 95% and 99% confidence levels, respectively. (C, D) TEM images of GP-phage@AuNPs internalized within PC3 cells in ultrathin section specimens. The cells were treated with GP-phage@AuNPs for 5 h, followed by medium replacement and additional incubation for 20 h.

function of the molar ratio of the number of AuNPs mixed with the phage to the total copy number of gold-binding peptides displayed on the phages (Figure 2D). The number of AuNPs per phage increased with the increased ratio of AuNPs to phages and reached a plateau value of about 70 per phage, which seem to be the saturation number as a highly packed assembly of AuNPs were observed in TEM images as shown in Figure 2E. We also examined the effects of the size of AuNPs on their binding capability to the phages. AuNPs of 10 and 25 nm in diameter were incubated with GP-phage in the same manner with 5 nm AuNPs. Although 10 nm AuNPs can bind to the phages despite much smaller number of AuNPs per phage (up to about 30 AuNPs per phage), 25 nm AuNPs hardly formed clusters on the surface of phages (Figure S2). These results indicate that the small size of AuNPs is important for efficient binding to T7 phages, which have a diameter of about 55 nm. We speculate that this size effect was derived from steric hindrance and a lower diffiusivity of larger AuNPs rather than any chemical differences of the surface of AuNPs. Further investigation is now underway to identify the factors involved in such size effects.

The hydrodynamic diameters of AuNPs, GP-phage, and GP-phage@AuNPs in phosphate buffered saline (PBS) were 9.6 ± 5.5 nm, 55.2 ± 3.3 nm, and 125.9 ± 14.4 nm, respectively (Figure S3). The zeta potentials of AuNPs and GP-phage were −17.81 ± 1.3 and −8.8 ± 1.1 mV, respectively. Interestingly, GP-phage@AuNPs became more negatively charged (− 34.78 ± 2.6 mV) (Figure S3). These results indicate that interactions between AuNPs and GP-phage are mediated not by electrostatic interations but by peptide-based specific interations. Electrostatic interactions have been widely used for preparation of nanoscale drug and gene carriers, but their structural stability often fails to be maintained by the presence of salts. Importantly, GP-phage@AuNPs showed good dispersion stability in a serum-containing medium. AuNPs and GP-phage@AuNPs in 10% fetal bovine serum (FBS) were incubated with shaking at 100 rpm at 37 °C. The hydrodynamic size of the particles was measured at predetermined time intervals (0, 3, 6, 12, and 24 h). There was no significant change in the particle size of GP-phage@AuNPs in PBS (125.9 ± 14.4 nm) and 10% FBS (129.9 ± 16.9 nm) (Figure S4). On the other hand, the size of citrate-stabilized AuNPs gradually

DOI: 10.1021/acsami.5b07029
ACS Appl. Mater. Interfaces 2015, 7, 22578−22586

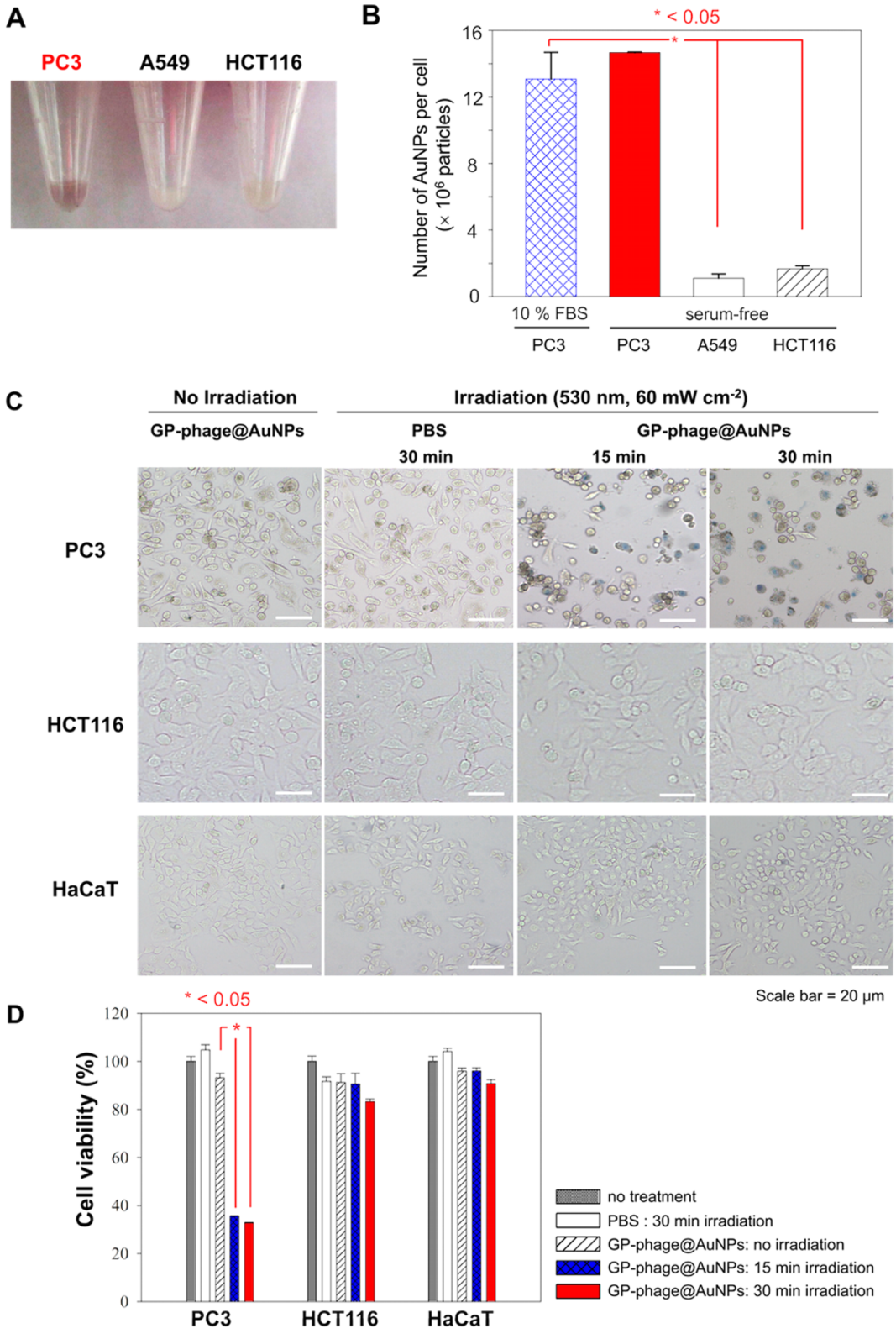

Figure 4. Prostate cancer cell-selective cellular uptake of GP-phage@AuNPs. (A) The photograph of the harvested cells treated with GP-phage@AuNPs. PC3 cells exhibited dark red due to the intrinsic color of AuNPs, whereas other cells did not. (B) The number of AuNPs bound on GP-phages internalized into each cell was measured using ICP-MS. (C) Blue staining of dead cells 3 h post irradiation. Each cells was treated with GP-phage@AuNPs and exposed to the light source (60 mW cm^{-2}) for 15 and 30 min. (D) The viability of each cell line by photothermal effects of GP-phage@AuNPs.

increased and were eventually aggregated to micrometer-sized precipitates in 6 h in 10% FBS. Their optical properties were also changed (Figure S4C, D). The excellent dispersion stability of GP-phage@AuNPs suggests that T7 phages-templated AuNP clusters are highly feasible for applications as a nanocarrier for targeted bioimaging and drug delivery.

DOI: 10.1021/acsami.5b07029
ACS Appl. Mater. Interfaces 2015, 7, 22578−22586

Cytotoxicity of the recombinant T7 phages and T7-templated AuNP clusters was determined using the lactate dehydrogenase (LDH) release assay. PC3 cells (7.0×10^3 cells/well) were incubated with GP-phage and GP-phage@AuNPs at 37 °C for 72 h in DMEM containing 10% FBS. No significant increase in the amount of LDH released to the media was found for all of the tested samples, indicating that they do not induce damage on the cell membranes (Figure S5A). In addition, cell viability was determined by the CCK-8 assay, which enables viable cells to be detected by a colorimetric method. Both GP-phage and GP-phage@AuNPs showed almost 100% cell viability up to 5.0×10^9 pfu/well in the cells. These results clearly verify that the recombinant phages and T7-templated AuNP clusters have no effects on the metabolic activities of cells (Figure S5B). Previous studies on the pharmacokinetics and immune responses of phages also suggest that phages do not cause any detrimental effects, implying that the use of phages is a possible approach to in vivo applcations.

To evaluate the specificity of receptor-mediated binding of GP-phage@AuNPs to PC-3 cells, we determined the numbers of GP-phage@AuNPs bound to and internalized into different types of cancer cells. PC3 (human prostate carcinoma), HCT116 (human colorectal carcinoma), and A549 (human lung carcinoma) were chosen for this purpose because all of them are epithelial cells originated from different organs. The cells were treated with GP-phage@AuNPs and harvested by centrifugation. The cell pellets collected from PC3 cells appear dark red color due to the SPR of AuNPs, whereas other cells did not exhibit the color (Figure 3A). The cellular uptake of GP-phage@AuNPs was also quantatively compared using inductively coupled plasma mass spectrometry (ICP-MS). The average number of AuNPs taken into individual cell was calculated by eqs 1 and 2 (see the Experimental Section). The quantitative assessment showed that the large number of AuNPs was markedly detected in PC3 cells treated with GP-phage@AuNPs compared to other cells, clearly demonstrating the target cell specificity of GP-phage@AuNPs (Figure 3B). The presence of serum did not significantly affect the cellular uptake of GP-phage@AuNPs as determined by ICP-MS (Figure 3B) and dark-field microscopy (Figure S6). There was also no significant change in the size distribution of GP-phage@AuNPs in 10% FBS, indicating good dispersion stability of the phage-templated AuNP clusters (Figure S4).

The target-specific interaction of GP-phage@AuNPs with PC3 cells was also examined on a dark-field microscope. Dark-field microscopy uses a narrow beam of white light and detects the scattered light by the nanoparticles, hence occurring brightly colored images of the nanoparticles against a dark background. Therefore, it has been known as a fast and sensitive way to imaging individual nanoparticles of 30 to 100 nm in diameter without staining.[39] In this study, the cells were incubated with three different recombinant T7 phages (G-phage, P-phage, and GP-phage) complexed with AuNPs at 37 °C for 4 h and washed to remove unbound AuNPs. Light-scattering images of the cells showed that GP-phage@AuNPs were distinctly visualized as bright spots (orange colored) on the target cells when compared to no significant signals from G-phage@AuNPs and P-phage@AuNPs incubated with the target cells (Figure 4A). Despite strong binding of AuNPs to G-phages, G-phage@AuNPs did not bind to the cells because of no targeting capability of the T7-templated AuNP clusters. In the case of P-phage, AuNPs did not simply bind to the recombinant phages because of the absence of the gold-binding peptide on the phages. These results clearly demonstrated that the tandem sequence display of both gold-binding and PC3-biding peptides is essential for targeted delivery of clustered AuNPs to cancer cells.

Quantitative analysis of GP-phage@AuNPs internalized into the cells was determined by direct elemental analysis of gold using ICP-MS. The average number of AuNPs internalized into an individual cell was calculated from eqs 1 and 2 (see the Experimental Section). When the cells were treated with GP-phage@AuNPs, AuNPs were accumulated in PC-3 cells more than 10 times compared to in other types of cells (Figure 4B). In addition, the distribution of AuNPs within the cells was observed by TEM, which enables direct visualization of metal nanoparticles inside the cells. For TEM observation, PC3 cells treated with GP-phage@AuNPs were fixed with glutaraldehyde and stained with osmium tetroxide, followed by dehydration. It is shown that large clusters of AuNPs were localized within vesicular organelles (e.g., endosomes) within the target cells. These results suggest that GP-phage@AuNPs were internalized via receptor-mediated endocytosis, generating a network structure of AuNP nanoclusters with a diameter of up to a few hundred nanometers (Figure 4C, D).

The clusterization of AuNPs and their intracellular localization can enhance photothermal effects to cause cell death under low-power-density irradiation.[27] In this sense, GP-phage can play as a multifunctional platform to effectively increase photothermal effects through the self-assembly of AuNPs to cancer-targeted T7 phages. We investigated the feasibility of GP-phage@AuNPs as an effective means of increasing cancer-targeted photothermal effects by treating three different cancer cells (PC3, HCT116, and A549) with GP-phage@AuNPs. The cells were then exposed to low-power visible light (530 nm, 60 mW cm^{-2}) for up to 30 min at 37 °C and incubated for additional 3 h without exposure to the light. After washing with PBS three times, the cells were stained with 0.4% trypan blue at 37 °C for 10 min and fixed with 4% formadehyde. The blue-stained cells were noticeably detected in the PC3 cells treated with GP-phage@AuNPs as an evidence of cell death, showing the target-specific photothermal effects under mild visible-light irradiation. On the other hand, any remarkable cell death was not observed in both of normal cells (HaCat) and non-targetable cancer cells (HCT116). The destruction of targeted cancer cells through photothermal effects of GP-phage@AuNPs were also confirmed by the Counting Kit-8 (CCK-8) assay, which determined cell viability by measuring the amount of the formazan dye generated by dehydrogenases in living cells. After irradiation, the cell viability of PC3 targeted by GP-phage@AuNPs was reduced to about 35% post irradiation for 15 min. On the other hand, HCT116 and HaCat cells maintained cell viability greater than 80 and 90%, respectively, under the same experimental condition. In PC3 cells, > 90% cell viability was observed for P-phage@AuNPs, G-phage@AuNPs, and citrate-stabilized AuNPs. The effects of the concentration of AuNPs on photothermal cytotoxicity were also examined for citrate-stabilized AuNPs and GP-phage@AuNPs (Figure S7). The cytotoxicity increased with the increased concentration of GP-phage@AuNPs while a much lower level of cytotoxicity was maintained even at a high concentration of citrate-stabilized AuNPs because of the dispersion instability of AuNPs as shown in Figure S4. The results suggest that only GP-phage@AuNPs induced selective and effective photothermal destruction of targeted cancer cells without significant damages to other cells.

DOI: 10.1021/acsami.5b07029
ACS Appl. Mater. Interfaces 2015, 7, 22578−22586

CONCLUSION

In conclusion, we suggested genetically modified T7 phages as a template to induce the self-assembly of AuNPs to nanoclusters for prostate cancer-targeted photothermal therapy. The major coat proteins of T7 phages were engineered to display both of a prostate cancer cell-binding peptide and a gold-binding peptide in a tandem sequence connected by a tetraglycine linker. The genetically modified T7 phages were simply mixed with AuNPs stabilized with citrates in an aqueous solution, leading to self-assembly of AuNPs into nanoclusters on T7 phages. The resulting prostate cancer-targeted, T7-templated AuNP nanoclusters (GP-phage@AuNPs) exhibited high dispersion stability in serum and no significant cytotoxicity. The AuNP nanoclusters were selectively targeted to prostate cancer cells, followed by the formation of entangled structures of the AuNP nanoclusters inside the cells. Under a low level of visible-light irradiation, the AuNP nanoclusters caused cell death in a very selective manner to prostate cancer cells. These results strongly suggest that the phage-templated approach can be a very promising route to efficient target-specific delivery of functional nanomaterials for therapeutic and bioimaging applications. We also expect that the T7 phage displaying the gold-binding peptide can be used for the self-assembly of gold nanorods, which can absorb the near-infrared light with a high photothermal conversion efficiency, enabling the in vivo applications of the T7-templated gold nanoclusters. Genetic modification of the T7 capsid proteins is very straightforward, making this approach easily applicable to a wide range of selective targeting to biomolecules and self-assembly of various molecules and nanomaterials.

METHODS

Materials. A T7Select 415−1 Cloning kit was purchased from Merck, Co. (Darmstadt, Germany). All components concerning growth media were purchased from BD Bioscience (Franklin Lakes, NJ, USA). HotStar Taq *plus* DNA polymerase was obtained from QIAGEN (Hilden, Germany). All primers for dsDNA inserts were synthesized from Bioneer Co. (Daejeon, Republic of Korea). PC3, HCT116, and A549 cell lines were obtained from the Korea Cell Line Bank (Seoul, Republic of Korea). A T4 DNA ligation kit, Rosewell Park Memorial Institute medium 1640 (RPMI-1640), Dulbecco's modified Eagle's medium (DMEM), PBS, and FBS were purchased from Invitrogen (Carlsbad, CA, USA). A CCK-8 assay kit was purchased from Dojindo laboratories (Kumamoto, Japan). AuNPs (5 nm in diameter) and a LDH assay kit were purchased from Sigma-Aldrich (St. Louis, MO, USA).

Construction of T7 Phage Displaying Target Peptides. To express Au-peptide, PC3-peptide, and both of them in tandem on the T7 phage capsid, the DNA sequences encoding the peptides were connected with a GGGG-linker (underlined). The sequences for Au-PC3-peptide were synthesized as follows: forward, 5′-[phosphate] AATT CA ATG CAT GGC AAA ACC CAG GCG ACC AGC GGC ACC ATT CAG AGC GGC GGC GGC GGC ATT GCG GGC CTG GCG ACC CCG GGC TGG AGC CAT TGG CTG GCG CTG-3′ and reverse, 5′-[phos] AGCT CAG CGC CAG CCA ATG GCT CCA GCC CGG GGT CGC CAG GCC CGC AAT GCC GCC GCC GCC GCT CTG AAT GGT GCC GCT GGT CGC CTG GGT TTT GCC ATG CAT TG-3′. The two primers were annealed at 95 °C for 3 min to form a dsDNA insert and ligated into a T7Select415−1b vector as prepared by EcoR I/*Hind* III digestion. The ligation reaction, in vitro packaging, and plaque assay were performed according to the T7Select system manual (Novagen, Merck KGaA, Darmstadt, Germany). DNA sequencing of the PCR products obtained using T7SelectUP and T7SelectDOWN primers was carried out to examine the inserted sequences of the recombinant T7 phages.

Clusterization of AuNPs to the Recombinant Phages. Ten microliters of the recombinant T7 phages (2×10^{11} pfu mL^{-1}) were incubated with 50 μL of AuNPs (5×10^{13} particles mL^{-1}) for 20 min. The mixtures were then centrifuged at 2,250 × g for 5 min to collect the AuNPs bound to the phages. The precipitates were resuspended in 100 μL PBS (10 mM Na_2HPO_4, 2 mM KH_2PO_4, and 156 mM NaCl), and their light-absorption spectra were measured using UV−vis spectrophotometry (UV-1800, Shimadzu, Kyoto, Japan).

TEM Analysis. A drop of samples were placed on 300-mesh copper TEM grids (Ted Pella, Inc., Redding, CA, USA) and allowed to be loaded for 20 min. The grids were then washed with deionized water three times and negatively stained with 1% uranyl acetate for 10 s. Images were taken using TEM (JEM-3011, JEOL Ltd., Tokyo, Japan).

Characterization of GP-phage@AuNPs. The recombinant phages (200 μL, 4×10^{11} pfu mL^{-1}) were incubated with 1 mL of AuNPs (5×10^{13} particles mL^{-1}) for 20 min. The particle sizes and zeta potentials were measured using DSL (ELSZ-1000, Otsuka Electronics Co., Ltd., Japan). The scattered light intensity was measured at a scattering angle of 165° at 25 °C, and the particle size was calculated using the CONTIN routine. Zeta potentials were measured in 1 mM PBS (pH 7.4). To determine the dispersion stability of GP-phage@AuNPs, we incubated the samples in 10% FBS with orbital shaking at 100 rpm at 37 °C for 24 h. The particle sizes of samples were measured at predetermined time intervals using DLS.

Cytotoxicity Assays. Cytotoxicity of the recombinant phages was investigated using the CCK8 assay and LDH release assays. PC3 cells were seeded onto a 96-well plate at a density of 7.0×10^3 cells/well to determine whether T7 phages have any cytotoxic effects on the cells. The cells were incubated with phages at concentrations from 5.0×10^8 to 5.0×10^9 pfu/well at 37 °C under 5% CO_2 for 72 h. Cell viability was determined from the absorbance of cells treated with the CCK8 solution at 450 nm using a plate reader (1420 Multilabel Counter, PerkinElmer). The supernatants were transferred to a new plate to perform LDH release assay using the absorbances at 490 and 690 nm.

Cancer Targeting. The cells were seeded in a chamber slide (4-well CultureSlides, BD Falcon) at a density of 7.0×10^4 cells/well and cultured in DMEM at 37 °C under 5% CO_2 for 24 h. The cells were treated with each recombinant T7 phage (2×10^9 pfu) mixed with AuNPs (2.5×10^{12} particles) at 37 °C for 4 h. The cells were washed with PBS three times, fixed with 1% formaldehyde, and then visualized on a dark-field microscope (Eclipse T*i*, Nikon). The amounts of AuNPs taken into PC3 cells were determined using ICP-MS. PC3, HCT116, and A549 cells were cultured onto a 6-well plate at a density of 1.0×10^6 cells/well at 37 °C under 5% CO_2 for 24 h. The cells were treated with each recombinant T7 phage (2×10^{10} pfu), which were mixed with AuNPs (2.5×10^{13} particles) at 37 °C for 5 h. After additional 20 h incubation, the cells were washed with PBS three times, harvested, and repeatedly washed with PBS. The harvested cells were pretreated with 70% nitric acid to degrade cell membranes before ICP-MS analysis. The numbers of AuNPs per cell were calculated by eq 1

$$N_{\mathrm{AuNP}} = \frac{N_{\mathrm{total}}}{N}\frac{1}{NC_{\mathrm{total}}} \tag{1}$$

where N_{total} is the total number of gold atoms within the cells, N is the average number of gold atoms per nanoparticle (N = 3862, calculated by eq 2),[40] and NC_{total} is the total number of treated cells. The norminal diameter of gold nanoparticles (D, nm) used in all experiments was 5 nm. ρ denotes the density for face centered cubic (fcc) gold (19.3 g cm^{-3}), M is the atomic mass of gold (197 g mol^{-1}), and N_A is the Avogadro number (6.02×10^{23}):

$$N = \frac{\pi}{6}\frac{\rho D^3}{M}N_{\mathrm{A}} \tag{2}$$

Intracellular Distribution of GP-phage@AuNPs. PC3 cells were seeded onto a 6-well plate at a density of 1.0×10^6 cells/well at 37 °C under 5% CO_2. The cells were treated with GP-phages (2×10^{10} pfu) mixed with AuNPs (2.5×10^{13} particles) for 5 h, followed by incubation in a fresh medium for 20 h. The cells were washed with

DOI: 10.1021/acsami.5b07029
ACS Appl. Mater. Interfaces 2015, 7, 22578−22586

PBS several times, fixed with 2.5% glutaraldehyde for 24 h, stained with 1% osmium tetroxide for 1 h, and then dehydrated. The samples were embedded in Epon812 and sliced as ultrathin sections for TEM analysis (Tecnai G2 Spirit, FEI).

Photothermal Effect of GP-phage@AuNPs on the Target Cells. PC3, HCT116, and HaCat cells were seeded onto a 96-well plate at a density of 2.0×10^4 cells/well and incubated at 37 °C under 5% CO_2 for 24 h. The cells were treated with GP-phages (2×10^8 pfu) mixed with AuNPs (2.5×10^{11} particles) and then incubated in a fresh medium for 20 h. The cells were exposed to a portable light-emitting diode (LED) light source for 15−30 min at 37 °C and incubated for additional 3 h. The LED has an emission peak of 530−540 nm and a power density of 60 mW cm^{-2}. The cells were washed with PBS several times, stained with 0.4% trypan blue at 37 °C for 10 min, fixed with 4% formaldehyde, and observed on an optical microscope (Leica Microsystems GmbH, Germany). The cell viability was determined by the CCK-8 assay. Cells were prepared in the same way described above. The cells were washed with PBS several times, reacted with media containing a CCK-8 assay solution, and then incubated at 37 °C under 5% CO_2 for 1 h. The absorbance was measured at 450 nm using a plate reader (1420 Multilabel Counter, PerkinElmer, Waltham, MA, USA).

■ ASSOCIATED CONTENT

Supporting Information

The Supporting Information is available free of charge on the ACS Publications website at DOI: 10.1021/acsami.5b07029.

Figures S1−S7 (PDF)

■ AUTHOR INFORMATION

Corresponding Author

*E-mail: yoonsung@kaist.ac.kr.

Notes

The authors declare no competing financial interest.

■ ACKNOWLEDGMENTS

This work was supported by the Korea CCS R&D Center (KCRC), Basic Science Research, and Nano·Material Technology Development Programs through the National Research Foundation of Korea (NRF) funded by the Ministry of Science, ICT & Future Planning (NRF- 2014M1A8A1049303, NRF-2013R1A1A1009626, and NRF-2012M3A7B4049802). We appreciate Prof. Ji Ho Park for insightful discussion and allowing us to use a dark-field microscope.

■ REFERENCES

(1) Casey, J. P.; Barbero, R. J.; Heldman, N.; Belcher, A. M. Versatile de Novo Enzyme Activity in Capsid Proteins from an Engineered M13 Bacteriophage Library. *J. Am. Chem. Soc.* **2014**, *136* (47), 16508−16514.

(2) Lee, Y.; Kim, J.; Yun, D. S.; Nam, Y. S.; Shao-Horn, Y.; Belcher, A. M. Virus-Templated Au and Au-Pt Core-Shell Nanowires and Their Electrocatalytic Activities for Fuel Cell Applications. *Energy Environ. Sci.* **2012**, *5* (8), 8328−8334.

(3) Nam, Y. S.; Magyar, A. P.; Lee, D.; Kim, J. W.; Yun, D. S.; Park, H.; Pollom, T. S.; Weitz, D. A.; Belcher, A. M. Biologically Templated Photocatalytic Nanostructures for Sustained Light-driven Water Oxidation. *Nat. Nanotechnol.* **2010**, *5* (5), 340−344.

(4) Nam, Y. S.; Park, H.; Magyar, A. P.; Yun, D. S.; Pollom, T. S.; Belcher, A. M. Virus-templated Iridium Oxide-gold Hybrid Nanowires for Electrochromic Application. *Nanoscale* **2012**, *4* (11), 3405−3409.

(5) Nam, Y. S.; Shin, T.; Park, H.; Magyar, A. P.; Choi, K.; Fantner, G.; Nelson, K. A.; Belcher, A. M. Virus-Templated Assembly of Porphyrins into Light-Harvesting Nanoantennae. *J. Am. Chem. Soc.* **2010**, *132* (5), 1462−1463.

(6) Brigati, J. R.; Petrenko, V. A. Thermostability of Landscape Phage Probes. *Anal. Bioanal. Chem.* **2005**, *382* (6), 1346−1350.

(7) Jepson, C. D.; March, J. B. Bacteriophage Lambda is a Highly Stable DNA Vaccine Delivery Vehicle. *Vaccine* **2004**, *22* (19), 2413−2419.

(8) Smith, G. P.; Petrenko, V. A. Phage Display. *Chem. Rev.* **1997**, *97* (2), 391−410.

(9) Pasqualini, R.; Ruoslahti, E. Organ Targeting In vivo using Phage Display Peptide Libraries. *Nature* **1996**, *380* (6572), 364−366.

(10) Oh, J. W.; Chung, W. J.; Heo, K.; Jin, H. E.; Lee, B. Y.; Wang, E.; Zueger, C.; Wong, W.; Meyer, J.; Kim, C.; Lee, S. Y.; Kim, W. G.; Zemla, M.; Auer, M.; Hexemer, A.; Lee, S. W. Biomimetic Virus-based Colourimetric Sensors. *Nat. Commun.* **2014**, *5*, 1−8.

(11) Jeong, C. K.; Kim, I.; Park, K. I.; Oh, M. H.; Paik, H.; Hwang, G. T.; No, K.; Nam, Y. S.; Lee, K. J. Virus-directed Design of a Flexible $BaTiO_3$ Nanogenerator. *ACS Nano* **2013**, *7* (12), 11016−11025.

(12) Lee, Y. J.; Yi, H.; Kim, W. J.; Kang, K.; Yun, D. S.; Strano, M. S.; Ceder, G.; Belcher, A. M. Fabricating Genetically Engineered High-Power Lithium-Ion Batteries Using Multiple Virus Genes. *Science* **2009**, *324* (5930), 1051−1055.

(13) Choi, D. S.; Jin, H. E.; Yoo, S. Y.; Lee, S. W. Cyclic RGD Peptide Incorporation on Phage Major Coat Proteins for Improved Internalization by HeLa Cells. *Bioconjugate Chem.* **2014**, *25* (2), 216−223.

(14) Newton, J. R.; Miao, Y. B.; Deutscher, S. L.; Quinn, T. P. Melanoma imaging with pretargeted bivalent bacteriophage. *J. Nucl. Med.* **2007**, *48* (3), 429−436.

(15) Jaye, D. L.; Geigerman, C. M.; Fuller, R. E.; Akyildiz, A.; Parkos, C. A. Direct Fluorochrome Labeling Of Phage Display Library Clones For Studying Binding Specificities: Applications In Flow Cytometry And Fluorescence Microscopy. *J. Immunol. Methods* **2004**, *295* (1−2), 119−127.

(16) Ghosh, D.; Lee, Y.; Thomas, S.; Kohli, A. G.; Yun, D. S.; Belcher, A. M.; Kelly, K. A. M13-templated Magnetic Nanoparticles for Targeted In vivo Imaging of Prostate Cancer. *Nat. Nanotechnol.* **2012**, *7* (10), 677−682.

(17) Yi, H. J.; Ghosh, D.; Ham, M. H.; Qi, J. F.; Barone, P. W.; Strano, M. S.; Belcher, A. M. M13 Phage-functionalized Single-walled Carbon Nanotubes as Nanoprobes for Second Near-Infrared Window Fluorescence Imaging of Targeted Tumors. *Nano Lett.* **2012**, *12* (3), 1176−1183.

(18) Ghosh, D.; Kohli, A. G.; Moser, F.; Endy, D.; Belcher, A. M. Refactored M13 Bacteriophage as a Platform for Tumor Cell Imaging and Drug Delivery. *ACS Synth. Biol.* **2012**, *1* (12), 576−582.

(19) Sakamoto, K.; Ito, Y.; Mori, T.; Sugimura, K. Interaction of Human Lactoferrin with Cell Adhesion Molecules through RGD Motif Elucidated by Lactoferrin-Binding Epitopes. *J. Biol. Chem.* **2006**, *281* (34), 24472−24478.

(20) Steven, A. C.; Serwer, P.; Bisher, M. E.; Trus, B. L. Molecular Architecture of Bacteriophage-T7 Capsid. *Virology* **1983**, *124* (1), 109−120.

(21) Steven, A. C.; Trus, B. L.; Maizel, J. V.; Unser, M.; Parry, D. A. D.; Wall, J. S.; Hainfeld, J. F.; Studier, F. W. Molecular Substructure of a Viral Receptor-Recognition Protein - the Gp17 Tail-Fiber of Bacteriophage-T7. *J. Mol. Biol.* **1988**, *200* (2), 351−365.

(22) Daniel, M. C.; Astruc, D. Gold Nanoparticles: Assembly, Supramolecular Chemistry, Quantum-size-related Properties, and Applications toward Biology, Catalysis, and Nanotechnology. *Chem. Rev.* **2004**, *104* (1), 293−346.

(23) Sau, T. K.; Rogach, A. L. Nonspherical Noble Metal Nanoparticles: Colloid-Chemical Synthesis and Morphology Control. *Adv. Mater.* **2010**, *22* (16), 1781−1804.

(24) Sanchez-Iglesias, A.; Pastoriza-Santos, I.; Perez-Juste, J.; Rodriguez-Gonzalez, B.; Garcia de Abajo, F. J.; Liz-Marzan, L. M. Synthesis and Optical Properties of Gold Nanodecahedra with Size Control. *Adv. Mater.* **2006**, *18* (19), 2529−2534.

(25) Huang, X. H.; Jain, P. K.; El-Sayed, I. H.; El-Sayed, M. A. Gold Nanoparticles: Interesting Optical Properties and Recent Applications

DOI: 10.1021/acsami.5b07029
ACS Appl. Mater. Interfaces 2015, 7, 22578−22586

in Cancer Diagnostic and Therapy. *Nanomedicine* **2007**, *2* (5), 681−693.
(26) Lee, U. Y.; Youn, Y. S.; Park, J.; Lee, E. S. Y-Shaped Ligand-driven Gold Nanoparticles for Highly Efficient Tumoral Uptake and Photothermal Ablation. *ACS Nano* **2014**, *8* (12), 12858−12865.
(27) Zharov, V. P.; Galitovskaya, E. N.; Johnson, C.; Kelly, T. Synergistic Enhancement of Selective Nanophotothermolysis with Gold Nanoclusters: Potential for Cancer Therapy. *Lasers Surg. Med.* **2005**, *37* (3), 219−226.
(28) Li, Y. Y.; Wen, T.; Zhao, R. F.; Liu, X. X.; Ji, T. J.; Wang, H.; Shi, X. W.; Shi, J.; Wei, J. Y.; Zhao, Y. L.; Wu, X. C.; Nie, G. J. Localized Electric Field of Plasmonic Nanoplatform Enhanced Photodynamic Tumor Therapy. *ACS Nano* **2014**, *8* (11), 11529−11542.
(29) Peceros, K. E.; Xu, X. D.; Bulcock, S. R.; Cortie, M. B. Dipole-dipole Plasmon Interactions in Gold-on-polystyrene Composites. *J. Phys. Chem. B* **2005**, *109* (46), 21516−21520.
(30) Nam, J.; Won, N.; Jin, H.; Chung, H.; Kim, S. pH-Induced Aggregation of Gold Nanoparticles for Photothermal Cancer Therapy. *J. Am. Chem. Soc.* **2009**, *131* (38), 13639−13645.
(31) Khlebtsov, B.; Zharov, V.; Melnikov, A.; Tuchin, V.; Khlebtsov, N. Optical Amplification of Photothermal Therapy with Gold Nanoparticles and Nanoclusters. *Nanotechnology* **2006**, *17* (20), 5167−5179.
(32) Brown, S. Metal-recognition by Repeating Polypeptides. *Nat. Biotechnol.* **1997**, *15* (3), 269−272.
(33) Whitesides, G. M.; Mathias, J. P.; Seto, C. T. Molecular Self-Assembly and Nanochemistry - A Chemical Strategy for the Synthesis of Nanostructures. *Science* **1991**, *254* (5036), 1312−1319.
(34) Sarikaya, M.; Tamerler, C.; Jen, A. K. Y.; Schulten, K.; Baneyx, F. Molecular Biomimetics: Nanotechnology through Biology. *Nat. Mater.* **2003**, *2* (9), 577−585.
(35) So, C. R.; Kulp, J. L.; Oren, E. E.; Zareie, H.; Tamerler, C.; Evans, J. S.; Sarikaya, M. Molecular Recognition and Supramolecular Self-Assembly of a Genetically Engineered Gold Binding Peptide on Au{111}. *ACS Nano* **2009**, *3* (6), 1525−1531.
(36) Braun, R.; Sarikaya, M.; Schulten, K. Genetically Engineered Gold-binding Polypeptides: Structure Prediction and Molecular Dynamics. *J. Biomater. Sci., Polym. Ed.* **2002**, *13* (7), 747−757.
(37) Schroder, F. H.; Hugosson, J.; Roobol, M. J.; Tammela, T. L. J.; Ciatto, S.; Nelen, V.; Kwiatkowski, M.; Lujan, M.; Lilja, H.; Zappa, M.; Denis, L. J.; Recker, F.; Paez, A.; Maattanen, L.; Bangma, C. H.; Aus, G.; Carlsson, S.; Villers, A.; Rebillard, X.; van der Kwast, T.; Kujala, P. M.; Blijenberg, B. G.; Stenman, U. H.; Huber, A.; Taari, K.; Hakama, M.; Moss, S. M.; de Koning, H. J.; Auvinen, A.; Investigators, E. Prostate-Cancer Mortality at 11 Years of Follow-up. *N. Engl. J. Med.* **2012**, *366* (11), 981−990.
(38) Newton, J. R.; Kelly, K. A.; Mahmood, U.; Weissleder, R.; Deutscher, S. L. In vivo Selection of Phage for the Optical Imaging of PC-3 Human Prostate Carcinoma in Mice. *Neoplasia* **2006**, *8* (9), 772−780.
(39) Orendorff, C. J.; Sau, T. K.; Murphy, C. J. Shape-dependent Plasmon-resonant Gold Nanoparticles. *Small* **2006**, *2* (5), 636−639.
(40) Liu, X. O.; Atwater, M.; Wang, J. H.; Huo, Q. Extinction Coefficient of Gold Nanoparticles with Different Sizes and Different Capping Ligands. *Colloids Surf., B* **2007**, *58* (1), 3−7.

DOI: 10.1021/acsami.5b07029
ACS Appl. Mater. Interfaces 2015, 7, 22578−22586